Oceanologia (2016) 58, 249—263

Available online at www.sciencedirect.com

ScienceDirect

journal homepage: www.journals.elsevier.com/oceanologia/

ORIGINAL RESEARCH ARTICLE

Satellite observations of seasonal and regional variability of particulate organic carbon concentration in the Barents Sea

Malgorzata Stramska [a,b,*], **Jagoda Bialogrodzka** [b]

[a] *Institute of Oceanology, Polish Academy of Sciences, Sopot, Poland*
[b] *Department of Earth Sciences, Szczecin University, Szczecin, Poland*

Received 20 November 2015; accepted 13 April 2016
Available online 4 May 2016

KEYWORDS
Barents Sea;
Satellite remote sensing;
Ocean color;
Particulate organic carbon

Summary The Nordic and Barents Seas are of special interest for research on climate change, since they are located on the main pathway of the heat transported from low to high latitudes. The Barents Sea is characterized by supreme phytoplankton blooms and large amount of carbon is sequestered here due to biological processes. It is important to monitor the biological variability in this region in order to derive in depth understanding whether the size of carbon reservoirs and fluxes may vary as a result of climate change. In this paper we analyze the 17 years (1998—2014) of particulate organic carbon (POC) concentration derived from remotely sensed ocean color. POC concentrations in the Barents Sea are among the highest observed in the global ocean with monthly mean concentrations in May exceeding 300 mg m^{-3}. The seasonal amplitude of POC concentration in this region is larger when compared to other regions in the global ocean. Our results indicate that the seasonal increase in POC concentration is observed earlier in the year and higher concentrations are reached in the southeastern part of the Barents Sea in comparison to the southwestern part. Satellite data indicate that POC concentrations in the southern part of the Barents Sea tend to decrease in recent years, but longer time series of data are needed to confirm this observation.

* Corresponding author at: Institute of Oceanology, Polish Academy of Sciences, Powstańców Warszawy 55, Sopot 81-712, Poland. Tel.: +48 58 73 11 600; fax: +48 58 55 12 130.
E-mail address: mstramska@wp.pl (M. Stramska).
Peer review under the responsibility of Institute of Oceanology of the Polish Academy of Sciences.

Production and hosting by Elsevier

http://dx.doi.org/10.1016/j.oceano.2016.04.004

1. Introduction

The Barents Sea (BS) is an Arctic shelf sea. It is an important region for monitoring climate change and interactions between the atmosphere, the sea ice, and the ocean. This sea with its area of about 10% of the Arctic Ocean and an average depth of about 230 m is in large part free of sea ice even during the winter season and has a great influence on the Arctic. This is because BS is located on the main pathway of the heat transported by the ocean from low to high latitudes (e.g., Ådlandsvik and Loeng, 1991; Beszczynska-Möller et al., 2012; Smedsrud et al., 2013). The heat is transported with the relatively warm Atlantic Water (Fig. 1a) by the Norwegian Atlantic Current (NAC). Near Tromsøflaket, a bank located at the entrance to the Barents Sea, the NAC splits into two branches. One branch flows eastwards into the Barents Sea, and the other one flows northwards to Spitsbergen and Fram Strait (e.g., Furevik, 2001). The inflow of AW into the BS takes place through the Barents Sea Opening (BSO, Fig. 1a). The AW is exposed in the BS to the cold air. It becomes chilled and vertically mixed (Maslowski et al., 2004; Rudels et al., 2004; Schauer et al., 2002, 2008). In addition, there is the Norwegian Coastal Water (NCW) flowing along the Norwegian coast and over the continental shelf as the Norwegian Coastal Current (NCC). The vertical and horizontal extent of the NCC varies seasonally, and the front between the NCW and AW is characterized by eddies and meanders.

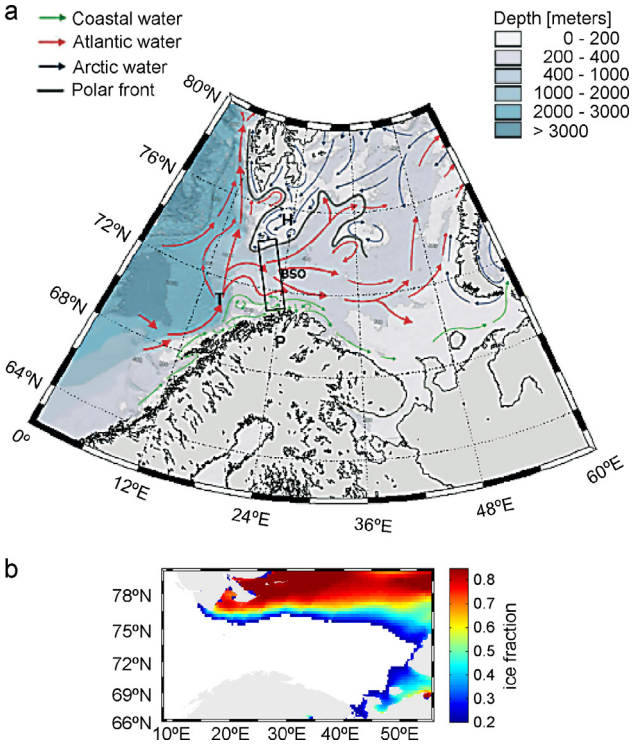

Figure 1 (a) Surface currents and bathymetry in the Barents Sea. Approximate position of the Barents Sea Opening (BSO) is indicated by a box, and letters T, H, and P indicate the location of Tromsoflaket, Hopen Island, and Porsangerfiorden. (b) The 33-year averaged (1982–2014) ice fraction in the study region in the month of May.

Tides are strong in the Barents Sea (the strongest in the Arctic apart from region near the Canadian Arctic Archipelago, Padman and Erofeeva, 2004) and they have substantial role affecting circulation and sea ice formation. Tidal mixing plays also a significant role for abyssal stratification and in controlling the water column structure on continental shelf. Interactions between tides and topography can stimulate topographic waves along the continental slope off the Northern Norway (Kowalik and Proshutinsky, 1995). This is an effective mechanism for cross slope exchange between the open sea and the shelf.

The atmospheric circulation over the BS is strongly influenced by cyclones advected from the North Atlantic. The strongest atmospheric pressure gradients are present in winter months, when southwesterly and westerly winds dominate in the southern part of the BS and southeasterly and easterly winds are frequently observed in the north (Terziev et al., 1990). The river runoff is small (163 km^3 $year^{-1}$) compared to other marginal seas of the Arctic Ocean. The Pechora River contributes most of the runoff (130 km^3 $year^{-1}$) (Lebedev et al., 2011).

Seasonal water mass transformations are driven by an intense vertical mixing due to cooling of the water masses over the entire Barents Sea in winter. In the Atlantic Water, the water column may become homogeneous down to 300 m due to vertical convection. Water mass transformations also include brine rejection processes caused by sea-ice formation in the northern and coastal BS (Schauer et al., 2002). In the spring, the water column stability in the Barents Sea is influenced by two mechanisms, ice melt and seasonal warming of the surface layer. Ice starts to melt in late April or early May, and a thin layer of melt water is progressively formed. This layer is usually more pronounced north of the Polar Front. Its thickness increases to 15–20 m during the summer and early autumn. The melt water surface layer is well-mixed and homogenous. In the Atlantic Water that is not covered by ice in winter, the stratification starts to develop when the sun begins to warm the surface layer. The stratification progresses very slowly. During summers a vertically homogeneous surface layer with about 10 m thickness is formed and some warming of the water can be observed down to 50–60 m. The Coastal Water along the Norwegian coast is, unlike the other main water masses in the Barents Sea, vertically stratified during the entire year. It preserves a weak vertical stability throughout the winter. In the spring and summer, the stratification increases because of the supply of fresh water and increased surface temperature.

It has been estimated that more than 50% of the Arctic Ocean winter heat loss occurs in the BS (Serreze et al., 2007). The oceanographic processes within the Barents Sea have a documented influence on the entire Arctic region and contribute significantly to the overall overturning in the Atlantic Ocean (Guemas and Salas-Melia, 2008; Semeneov et al., 2009). It has been shown that the Nordic and the Barents Seas are a significant sink for atmospheric carbon dioxide throughout the year (about 20–85 g C m^{-2} $year^{-1}$), while the export production due to biological productivity is in the range of 15–75 g C m^{-2} $year^{-1}$ (Skjelvan et al., 2005; Wassmann et al., 2006). Because there is a significant production of the dense (cold and salty) waters, the carbon contained in these waters can be sequestered for hundreds of years when the waters flow into the neighboring deep basins

of the Nordic Seas and Arctic Ocean (Dmitrenko et al., 2015; Lien and Trofimov, 2013; Lien et al., 2013). This means that the Barents Sea is an important region for studying ocean carbon cycle. Recently a comprehensive regional carbon budget has been constructed for the Barents Sea (see Kivimäe et al., 2010 and the references therein). This budget has been based on modeled volume flows and in situ data on dissolved inorganic carbon (DIC), dissolved organic carbon (DOC), and particulate organic carbon (POC) concentrations. The authors quantified many aspects of the regional carbon budget including fluxes due to advection, river and land sources, total CO_2 air–sea exchange, extra uptake of CO_2 in the polynyas, and burial in the sediments. One of the biggest uncertainties in the budget has been attributed to the variability of biological production and limited knowledge about spatial distribution and temporal variability of POC and DOC concentrations. An additional information about these quantities can be gained through ocean color remote sensing, which can complement in situ measurements.

The main goal in the present paper is to document spatial and temporal variability of POC concentrations in the surface waters of the Barents Sea using available satellite ocean color data. In particular we analyze the 17 years (1998–2014) time series of POC concentrations derived from data collected by the Sea-viewing Wide Field-of-view Sensor (SeaWiFS) aboard the OrbView-2 satellite and the Moderate Resolution Imaging Spectroradiometer deployed on the Aqua (EOS PM) satellite (MODIS-A). The BS is in large part ice-free all year round, thus permitting satellite observations of ocean color. Satellite POC data have been shown to have a similar performance as the chlorophyll data (Świrgoń and Stramska, 2015) and have been used to quantify particulate organic carbon reservoirs in different regions of the global ocean (e.g., for global estimates see Duforêt-Gaurier et al., 2010; Gardner et al., 2006; Stramska and Cieszyńska, 2015). Recall that POC particles include all living (e.g., phytoplankton, zooplankton) and non-living (e.g., detritus, fecal pellets) particles that contain organic carbon. The main source of POC particles in the open ocean is primary production. The information about variability and trends in POC biomass in the ocean can improve research on oceanic biological pump and its role in the sequestration of atmospheric carbon.

Satellite images of ocean color indicate that in the Barents Sea concentrations of POC reach impressively high values, and undergo significant interannual and regional variability. We will describe characteristic features of this variability, and investigate if this variability can be related to physical properties of the region, such as the sea surface temperature (SST), sea level anomalies (SLA), wind stress and ocean-atmosphere heat fluxes. We expect to find significant dependencies because phytoplankton blooms in the northern North Atlantic have been linked in the past to physical processes through in situ observations (e.g., see Marra et al., 2015, and the references therein), satellite data (e.g., Stramska, 2005) and phytoplankton models (e.g., Fasham et al., 1990; Stramska and Dickey, 1994; Stramska et al., 1995; Sverdrup, 1953; Tett and Edwards, 1984). Phytoplankton growth depends on available sunlight, water temperature, and nutrient availability. This can have important consequences for seasonal and climate related changes, and correlations in geographical patterns of SST and Chl.

The dependencies between mixing and phytoplantkton dynamics are different in different geographic regions. In the northern North Atlantic they can be summarized as follows (e.g., Stramska, 2005). (1) In winter/early spring there is enough nutrients in surface waters and there may be significant light energy at the top of the water column, but phytoplankton do not remain long enough near the surface to make significant growth. This is because water is being mixed over the mixed layer depths (MLD), which is relatively deep at this time of the year. (2) With the start of the seasonal stratification in spring and early summer, there are enough nutrients and light to support phytoplankton growth and initiation of phytoplankton bloom. It is an increased stabilization of the water column (increased SST) that allows phytoplankton to exploit higher irradiance intensities near the surface in early spring. Primary productivity increases and losses of biomass due to transport by mixing to deep waters decrease in comparison to the situation before bloom initiation. Therefore it seems that at this early phase of the phytoplankton bloom, there should be a positive correlation between SST and the biomass concentration in surface waters. Increased mixing of the water column will lead to decrease of the SST and of phytoplankton biomass in surface waters. This scenario has been supported in the past by in situ observations in the North Atlantic (see Marra et al., 2015, and the references therein). (3) In contrast, later in the season when waters are stratified, there is enough light but not enough nutrients to support net growth, and phytoplankton biomass decreases with increased stratification. At this stage we can expect that the warmer the surface water becomes in a given region (greater SST), the less mixing there is between surface and deeper, more nutrient-rich water. As surface water warms, the stratification becomes more pronounced, suppressing mixing and decreasing a transfer of nutrients from deeper to surface waters. Therefore phytoplankton productivity declines, and we would expect a negative correlation between SST and phytoplankton biomass in surface waters during this time of the year.

Regarding the long-term response of ocean productivity to rising temperatures (Henson et al., 2010), ocean models predict that increased SST will enhance stratification of the upper oceans (e.g., Hofmann et al., 2011), reducing the depth of the mixed layer and decreasing nutrient exchange with the deep ocean. Remote-sensing derived, globally averaged Chl *a* showed a significant negative relationship with density differences in the upper oligotrophic open ocean (Behrenfeld et al., 2006). Spatial patterns on a basin-scale for the stratified North Atlantic Ocean with SST ranging between 13 and 23°C are characterized by a strong inverse relationship between phytoplankton productivity and biomass with SST, mainly because nutrient supply is diminished in regions with higher SST (e.g., van de Poll et al., 2013).

2. Data sources and methods

Satellite remote sensing makes it possible to acquire large scale information about the oceans including dangerous and inaccessible regions. One such region is the Arctic, where temporal and spatial distribution of in situ observations has been irregular and insufficient, because of the inhospitable

conditions and harsh weather. Therefore, satellite remote sensing is a method of particular importance in the Arctic research. This article is based on analysis of interdisciplinary satellite data obtained from different sources for an important province of the Arctic, the Barents Sea. Our goal is to provide consistent description of POC concentration variability. Since the northern part of the Barents Sea is to a varying extent covered by sea ice (Fig. 1b), our analysis is more focused on the southern parts of the Barents Sea. To examine the correlations between different quantities, standard statistical methods have been used. Simple linear model for trends has been assumed, fitted to selected time series by a least square method and tested for statistical significance (Bendat and Piersol, 2010).

2.1. Ocean color data

The primary data set used in this study includes daily ocean surface POC concentrations derived from ocean color data collected by SeaWiFS and MODIS-Aqua. Each of these satellite missions provided global coverage of remote sensing reflectances in selected spectral bands in the visible and near-infrared spectral regions at approximately every 2 days (e.g., Franz et al., 2007; Siegel et al., 2013). Data have been processed by NASA using standard procedures (Franz et al., 2007; O'Reilly et al., 1998, 2000). These procedures involve atmospheric correction and removal of pixels with land, ice, clouds, or heavy aerosol load prior to calculation. For our study we have downloaded Level 3 POC data (Standard Mapped Images, SMI) with a nominal 9.2 km resolution at the equator, reprocessing versions R2010.0 and R2013.1 of SeaWiFS and MODIS-A data, respectively. This POC data product is derived by NASA with Stramski et al. (2008) algorithm, that allows to calculate POC concentrations from blue-to-green remote sensing reflectance band ratio. Comparisons of simultaneous satellite and in situ POC determinations in the global ocean can be found in Świrgoń and Stramska (2015). Approach to POC data analysis in the present study is similar to that described in Stramska (2014) and Stramska and Cieszyńska (2015). Therefore, we provide only a brief overview of these methods.

Daily POC concentrations [mg m^{-3}] were converted to the 21-day moving averages to fill in the missing data. At present it is difficult to precisely estimate the impact of data gaps due to clouds on average POC estimates presented on our maps. However, Racault et al. (2014) indicate that increased number of missing data in CZCS record in comparison to SeaWiFS has relatively low impact on quantities such as seasonal or annual mean chlorophyll concentrations. The estimates of the date of initiation of spring phytoplankton bloom or the duration of the growing season are more sensitive to gaps in ocean color data (Cole et al., 2012; Racault et al., 2014). Therefore we have limited our discussion to regional and seasonal means. From 21-day averaged data we estimated the monthly, annual, and the 17-year averaged POC concentrations. Data presented as spatial averages (including time series plots) represent the weighted averages from all pixels within the selected region. The weighted average accounts for the fact that pixel area at given latitude is equal to the cosine of this latitude multiplied by the pixel area at the equator (Campbell et al., 1995). The four regions, subjectively defined to show example time series of spatially averaged POC concentrations, are indicated in Figs. 2 and 5 as black boxes. The exact positions of these regions do not have any special significance, the regions have been defined mainly to illustrate temporal patterns of POC variability. We are interested in large-scale patterns, and using regional averages allows us to filter out the smaller scale variability. The geographical limits for each of the regions are as follows: region 1: 10.125–18.125°E and 71.375–74.375°N; region 2: 23.125–35.875°E and 72.0–75.0°N; region 3: 38.375–48.125°E and 69.375–72.875°N; region 4: 25.0–27.3°E and 70.95–71.45°N. For brevity we will use in this paper terms such as 'region 1 averages' or 'regional averages'. In all cases the regional averages were calculated only from pixels representing ocean surface. In the final POC dataset, data in years 1998–2002 are from SeaWiFS, in 2003–2007 represent average daily POC concentrations from SeaWiFS and MODIS-A, while in 2008–2014 are from MODIS-A observations. Estimates of multiyear trend in POC concentrations are based on data from one sensor (MODIS-A from 2003 to 2014) to avoid issues related to sensor intercalibrations.

Some of our results highlight seasonal POC variability in coastal waters. In coastal waters the standard NASA algorithms generally can be associated with increased errors in comparison to open oceans, because of optically more complex water composition (e.g., Woźniak, 2014; Woźniak et al., 2011). This is why we have decided to present additionally ocean color estimates of the vertical diffuse attenuation coefficient at 490 nm ($K_d(490)$). In this case $K_d(490)$ has been derived with the so called QAA algorithm (Lee et al., 2005a, b, 2007). The QAA algorithm has been validated in a wide range of oceanic and coastal regions and has been shown to have acceptable performance in optically complex waters (e.g., Doron et al., 2007; Lee et al., 2005a, 2007). Note that strictly speaking the vertical attenuation coefficient, $K_d(\lambda, z)$ is not a property of the water itself, but rather a descriptor of the underwater light field. It varies with depth and solar altitude (e.g., Mobley, 1994; Stramska and Frye, 1997). However in many studies $K_d(\lambda)$ has been treated as a quasi inherent optical property (quasi-IOP), because experimental data and inverse radiative transfer modeling efforts have shown that $K_d(\lambda)$ is strongly correlated with inherent optical properties, IOPs (see Kirk, 1984, 1991; Mobley, 1994). Thus, it is important to keep in mind that the spectral vertical attenuation coefficient ($K_d(\lambda)$) is significantly influenced by the variable concentrations of phytoplankton, colored dissolved organic matter (CDOM), and other optically active water components.

2.2. Sea surface temperature (SST) data

To illustrate regional variability and trends in sea surface temperature (SST) we have used the 33 years long data series (years 1982–2014) known as the National Oceanic and Atmospheric Administration (NOAA) Optimum Interpolation SST Version 2 data set (Reynolds et al., 2007). These SST data were provided by the NOAA/OAR/ESRL PSD, Boulder, Colorado, through their website at http://www.esrl.noaa.gov/psd/. These are daily records with spatial resolution of $0.25^\circ \times 0.25^\circ$, derived from the Advanced Very High Resolution Radiometer (AVHRR) infrared satellite measurements (Pathfinder data: from September 1981 to December 2005;

operational AVHRR: January 2006 onwards). In situ data from ships and buoys were used for a large-scale adjustment of satellite biases with respect to the in situ data, before data delivery by NOAA as the research quality data set. More details of the data processing methods can be found in Reynolds et al. (2007). Before applying the correction for bias, the satellite data have been classified into daytime and nighttime bins and they were corrected separately. Then, all the data have been reanalyzed jointly using the optimum interpolation (OI) procedure. The final data set represents the daily mean SST values and includes complementary information about the total SST error and information about ice fraction in a given pixel. Ice fraction equals 0 if there is no ice and equals 1 if sea surface is completely covered by sea ice. NOAA OISST SST data are currently the longest satellite data record that can be used to study long-term SST variability and trends. Note that the infrared satellite remote sensing SST algorithms can provide either a skin SST if they are based on radiative transfer models or a subskin SST if in situ observations have been used to adjust satellite retrievals (Merchant and LeBorgne, 2010). In the NOAA OI SST Version 2 data, the bias correction of the satellite data has been based on data from ships and buoys, therefore it can be interpreted as the bulk SST at about 0.5 m depth (Reynolds et al., 2007).

2.3. Sea level anomaly (SLA) data

To characterize the variability of sea level we have used sea level anomalies (SLA) extracted from the delayed time (DT) multimission global gridded data product available at AVISO (www.aviso.oceanobs.com). The SLA data are continuously updated by AVISO and referenced to the 20-year (1993–2012) mean sea surface height. For this study we have used the available DT SLA data, covering the time period from January 1, 1993 to December 31, 2014 (22 years). The SLA data have been interpolated by AVISO on $0.25^\circ \times 0.25^\circ$ spatial grid with 1-day temporal resolution, using computing methods based on objective analysis. Data have been corrected for instrumental noise, orbit determination error, atmospheric attenuation (wet and dry tropospheric and ionospheric influences), sea state bias, and tidal influence. The tidal aliasing is routinely corrected for by using tidal models that assimilate altimetry data (Le Provost, 2001). Detailed information about standard data processing methods is available at www.aviso.oceanobs.com. The error in the SLA data estimated by AVISO is about 1–2 cm. A comprehensive validation of a gridded satellite altimetry data product in the high-latitude seas, including the Barents Sea has been published by Volkov and Pujol (2012). The altimetric sea level determinations in coastal areas have been compared with available tide gauge records showing a good agreement in terms of the root-mean square differences, the amplitudes and phases of the seasonal cycle, and the long-term trend. Away from the coast the altimetry data have been found consistent with the mesoscale variability derived from drifter data.

2.4. Meteorological and hydrography data

To evaluate the role of atmospheric forcing we have used the meteorological data from the NOAA-CIRES Climate Diagnostic Center NCEP/NCAR (National Centers for Environmental Prediction and National Center for Atmospheric Research) Reanalysis 2. These data sets are based on state-of-the-art analysis/forecast system to assimilate global meteorological data from various available sources from 1948 to the present. In particular we have used the daily latent and sensible heat flux estimates, along with the net longwave and net shortwave radiation estimates to calculate the net heat flux at the sea surface. We have also used the wind stress data.

To discuss water properties we have used the World Ocean Atlas data (WOA 2013 version 2, www.nodc.noaa.gov/OC5/woa13/) provided by the National Ocean and Atmospheric Administration (NOAA) National Centers for Environmental Information (NCEI). The WOA consists of a climatology of fields of in situ ocean properties objectively analyzed for the World Ocean (Boyer et al., 2013). We have downloaded (1° grid) climatological monthly means of in situ temperature, salinity, and nitrate.

3. Results

3.1. Regional trends in SST and SLA

We start with a brief description of environmental conditions characterizing our study region. Fig. 2a and b shows the regional distribution of the 33-year averaged annual and May SST, respectively. Spatial SST distributions presented in Fig. 2a and b demonstrate significant influence of surface patterns of major oceanic currents shown in Fig. 1. The highest values of the 33-year average annual and May SST (about 8°C) are noted in the Norwegian Atlantic Current (NAC), while the lowest SST values (below 0°C) are detected in the northeastern part of the Barents Sea, a region which is covered by sea ice in winter. In Fig. 2c we have displayed spatial distribution of the 33-year averaged amplitude of the annual SST cycle. As can be seen in Fig. 2c the greatest amplitude of the seasonal SST cycle (about 8°C and more) is associated with the southeastern regions of the Barents Sea. These include regions located near Norway, within the shallower section of the Barents Sea where the water depth is below 300 m (compare with Fig. 1). The smallest amplitude of the 33-year averaged annual SST cycle ($\sim 3^\circ$C) is observed in the northern regions and in the West Spitsbergen Current. In Fig. 2d we have plotted spatial distribution of the standard deviations (STD) calculated from the 33-years long time series of the daily SST. These STDs were estimated after subtracting from the daily SST data the seasonal cycle and the multi-year trend. Thus, Fig. 2d illustrates the overall spatial variability of SST, unrelated to the seasonal cycle and multi-year trend. Note that the highest STD values (about 1.4°C) are documented near the Svalbard Archipelago and between Novaya Zemlya and the coastal regions near Russia. These high STD values can be due to the variable position of surface currents and frontal zones. The lowest STDs ($\sim 0.7^\circ$C) are associated with the AW inflow in the southwest part of our study region and are also observed in the northeastern region.

Time series of annually averaged SST data allowed us to estimate the 33-year annual and May SST trends, displayed in Fig. 2e and f. From the results shown in Fig. 2e and f it is clear that the trends (statistically significant at 95% confidence

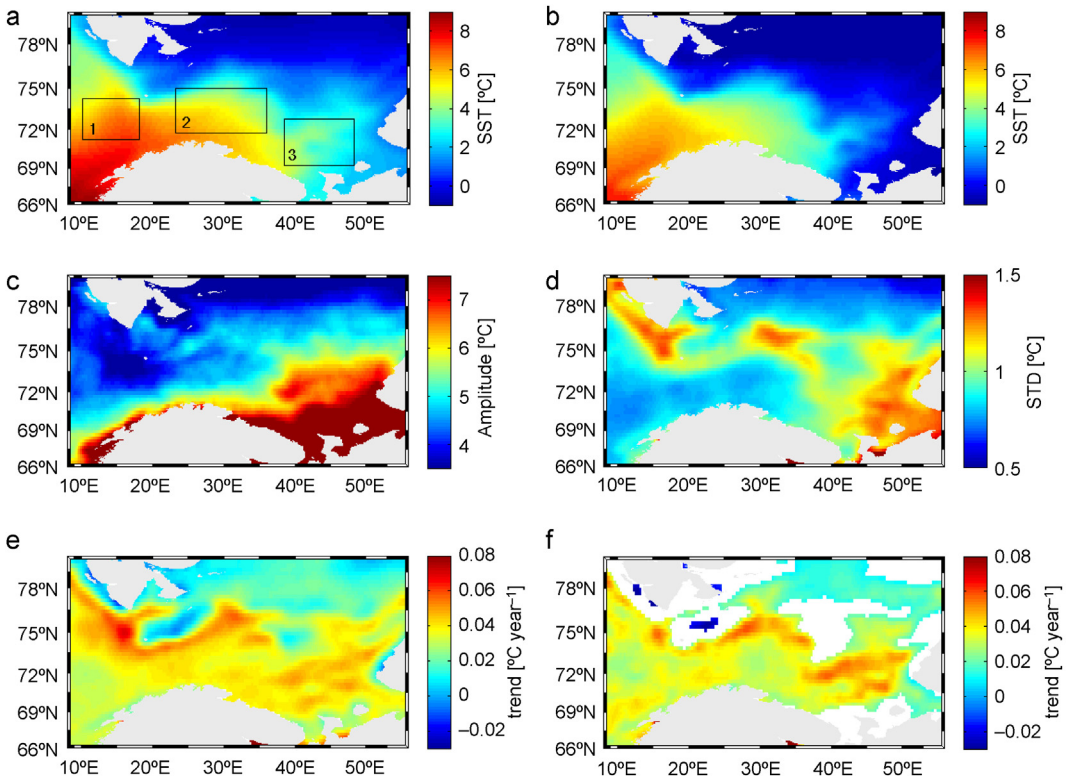

Figure 2 Maps based on the 33 years of SST data (1982–2014): (a) the 33-year mean SST, (b) the 33-year mean SST in the month of May, (c) the 33-year mean amplitude of the annual cycle, (d) standard deviation of SST anomalies, (e) trends in the annual mean SST, and (f) trends for the monthly mean SST in May. Only pixels with statistically significant ($p < 0.05$, 95% confidence level) trend have been displayed. Black boxes indicate study regions 1, 2, and 3 (see explanations in Section 2).

level, $p < 0.05$) of increasing annual and monthly mean SST (for the month of May) are detected in most of the area of the southern Barents Sea. Trends assume values of about 0.06°C year^{-1} (i.e., 0.6°C per decade) in the regions located west of the Hopen Island and between 0.04 and 0.06°C year^{-1} near the coastal regions off Norway. The trends in annually averaged SST are low or insignificant in the northern regions of the Barents Sea. Larger values of SST trend in the southern BS can be related to an increase of the volume and temperature of the Atlantic Water transported into the Barents Sea (Årthun et al., 2012). Recently, Oziel et al. (2016) showed that the volume of the Atlantic Water had approximately doubled between 1980 and 2011, and the domain occupied by the Atlantic Water extended further east and north. The authors indicate that although in the western part of the BS, the position of the Polar Front is constrained by the topography, in the eastern BS the position of the Southern Front (temperature front) is moving northward.

For comparison, according to Morice et al. (2012) linear trends in global surface temperature anomalies from 1979 to 2010 are approximately 0.17°C per decade, while northern/southern hemispheric trends are 0.24/0.10°C per decade. Luo et al. (2011) estimated linear trends for global, terrestrial, and ocean surface air temperatures (SAT) from 1982 to 2008 as 0.14, 0.21, and 0.10°C per decade, respectively. Using the 20 years (from January 1985 to December 2004) of the global Advanced Very High Resolution Radiometer Pathfinder data, the global SST trend has been estimated to be 0.18 and 0.17°C per decade based on the daytime or nighttime data respectively (Good et al., 2007). The warming trends estimated by us in the Barents Sea are greater than these global trends in most of the region located south from 76°N (see also Jakowczyk and Stramska, 2014).

Satellite altimetry sea level anomaly (SLA) data covering 22 years (1993–2014) have been used to investigate sea level variability in the study region. We have estimated regional pattern of statistically significant (95% confidence level, $p < 0.05$) trend in sea level (Fig. 3a). This trend varies spatially with values of about 2–4 mm year^{-1} in the southern Barents Sea. Similar trends for this region have been estimated before by Volkov and Pujol (2012), based on somewhat shorter SLA data record, covering the time from December 1992 to November 2010. For comparison, according to Nerem et al. (2010), the rate of globally averaged sea level rise is estimated currently as 3.1 mm year^{-1} (or 3.4 mm year^{-1} if correction for global isostatic adjustment is taken into account). Similar estimate of the global trend has been published by the Commonwealth Scientific and Industrial Research Organization (CSIRO, 3.2 mm year^{-1}, see www.cmar.csiro.au/sealevel/sl_hist_last_15.html), and by AVISO (3.2 mm year^{-1}, see www.aviso.oceanobs.com/en/news/ocean-indicators/mean-sea-level/). Thus, the sea level trend in the coastal regions of the southern Barents Sea is slightly higher than the globally averaged trend derived from satellite altimetry data. In Fig. 3b we have plotted standard deviation estimated from detrended SLA data. This result shows that the sea level variability is strongest in the southeastern Barents Sea. Note that this is almost the same region

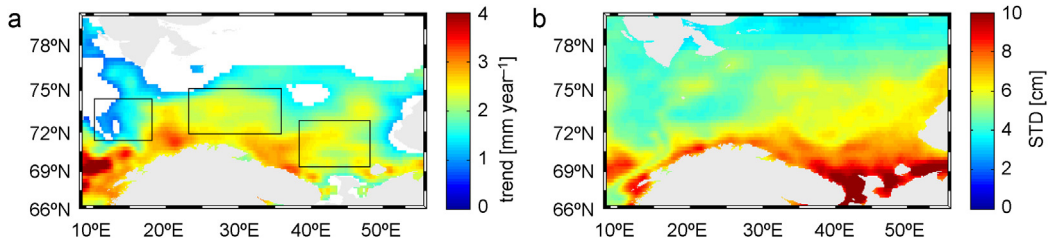

Figure 3 Sea level variability: (a) the 22-year trend (1993–2014) in the SLA data record. Only pixels with statistically significant ($p < 0.05$, 95% confidence level) trend have been displayed. (b) Standard deviations in the SLA data.

where we have observed relatively large annual amplitude and standard deviations of SST values (see Fig. 2).

It has been shown before that the major component in the variability of the altimetric and tide gauge sea level records in the BS region is the seasonal cycle (Volkov and Pujol, 2012). Its annual amplitude varies from about 7 to over 10 cm along the Norwegian coast. It has been confirmed by Volkov et al. (2013) that the sea level mass related variability in the central part of the BS is due to the combined effect of wind forcing balanced by the flow over the varying bottom topography (topographic influence). According to these authors wind forcing is the main reason for the observed time lag between the annual maxima in the Norwegian and Barents Seas.

3.2. POC concentrations

Maps displayed in Fig. 4 are summarizing the spring/summer variability of POC concentrations in the study region and show the 17-year averaged monthly data. The variability due to seasonal cycle is significant. The highest POC concentrations (more than 300 mg m^{-3}) can be found in the region located south from 76°N and between 22–50°E in May. West from about 22°E, at the edge of the Barents Sea and in the vicinity of the Norwegian Sea, the maximum annual POC concentrations are observed later in the year (in June), and on average these concentration do not reach as high values as they do in the region east from 22°E in May. It should be noted that the 17-year averaged POC monthly mean concentrations in the Barents Sea achieve quite high values when compared to global averages (see Stramska and Cieszyńska, 2015 for global estimates). For example it has been shown that the maximum seasonal POC concentration averaged over the entire North Atlantic Ocean is only about 110 mg m^{-3} and the annual mean is ~90 mg m^{-3}. The maximum values in different parts of the northern North Atlantic can exceed 300 mg m^{-3}. The Barents Sea is one of the few regions of the global ocean where such extreme values are regularly observed in satellite data.

When analyzing the characteristic features of POC concentration variability in the Barents Sea, we have noted that the temporal patterns of POC concentrations in the coastal regions off Norway are not synchronized with the progression of the seasonal cycle in the open waters of the southern Barents Sea. To show this in a better focus we present in Fig. 5 maps of monthly POC concentrations and vertical diffuse attenuation coefficient for downwelling irradiance at 490 nm (K_d(490)). We understand that ocean color POC estimates in coastal waters

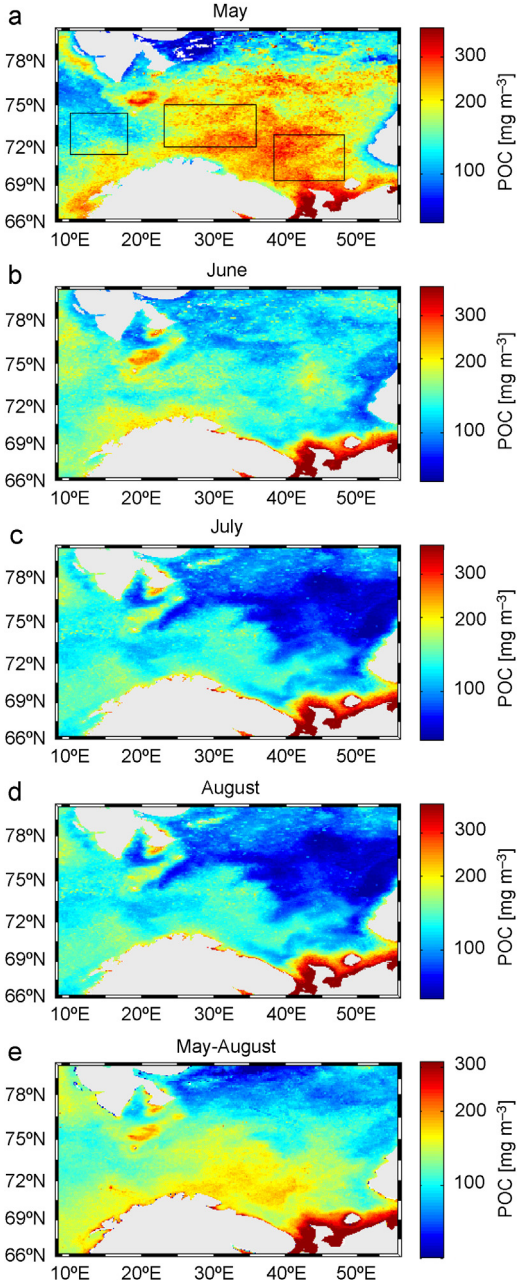

Figure 4 Maps of the 17-year averaged (1998–2014) surface POC concentrations in (a) May, (b) June, (c) July, (d) August, and (e) in summer (May–August).

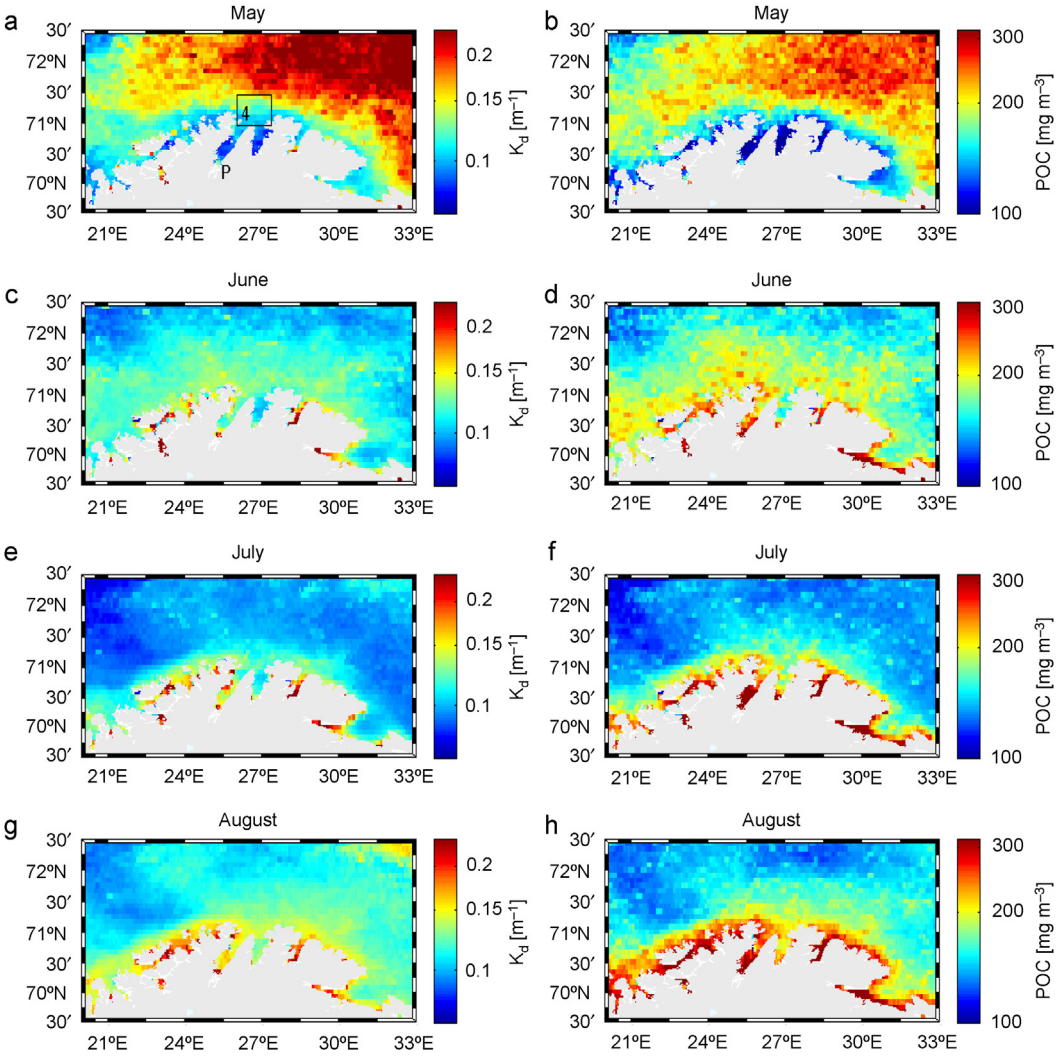

Figure 5 Maps of the 17-year averaged (1998–2014) (left panel) vertical diffuse attenuation coefficient at 490 nm, $K_d(490)$; (right panel) the monthly mean surface POC concentrations in the months of (a and b) May, (c and d) June, (e and f) July and (g and h) August. Black box in figure a indicates region 4.

may include larger errors than in the open ocean waters, but both $K_d(490)$ and POC estimates shown in Fig. 5 strongly suggest that in May coastal waters are characterized by rather low concentrations of optically active water components in comparison to the open ocean waters. These concentrations increase in coastal waters in June and in July. In August coastal waters are significantly more turbid than the open waters. A more quantitative interpretation of ocean color satellite data in coastal waters is out of scope if this paper, as coastal waters require a special approach including validations of local ocean color algorithms. We have recently carried out in situ experiments in one of the fjords shown in Fig. 5 (Porsangerfiorden) and we will address these problems in our next paper.

In order to stress the regional differences in seasonal cycles, we present in Fig. 6 the 17-year averaged daily time series of SST and POC concentrations averaged in the study regions 1, 2, 3, and 4. Region 1 is associated with the smallest amplitude of the seasonal SST cycle and the highest annual average SST value (Fig. 6a). The largest annual SST amplitude is observed in region 3. The differences between the 17-year averaged regional daily SST values in these two regions are more pronounced in the winter than in the summer. The SSTs in the winter season in coastal waters (region 4) have similar values as in region 2 but in the summer the SSTs in region 4 reach higher values than in region 1. In Fig. 6b we compare the time progression of the seasonal POC cycle in each of the regions. Since ocean color satellite data are missing due to low solar angles in winter, we limited this comparison to the time period of April through September. In Fig. 6b we can see that the rapid seasonal increase in POC concentration is observed on average earlier in the year and the maximum POC concentrations reach higher values in regions 2 and 3 than in regions 1 and 4. The seasonal progression of the cycle is similar in regions 2 and 3. Significant seasonal increase of POC concentration in region 2 and 3 is observed on average around year day 100 and it is accompanied by only a small increase in SST. Maximum SST values in the annual cycle are observed significantly later in the year (August) than the maximum POC concentrations (May). In comparison to regions 2 and 3, the seasonal increase in POC concentrations in region 1 is observed on average later in the year (days 115–125), the maximum concentrations are reached in June

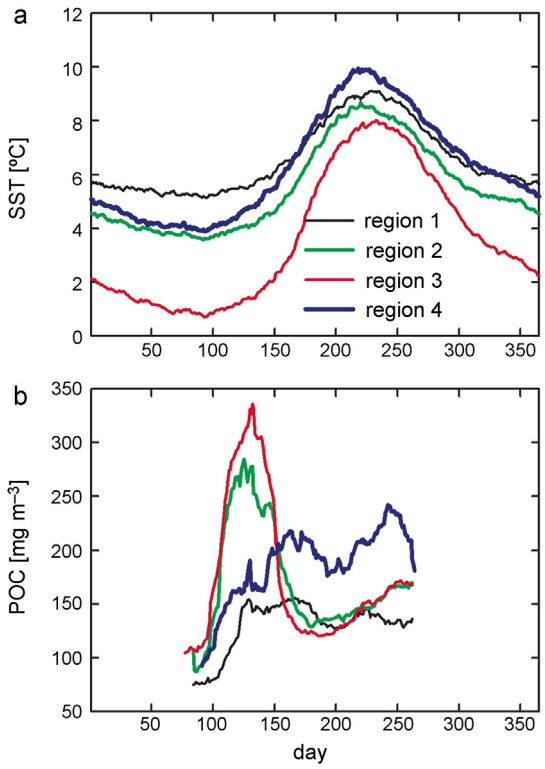

Figure 6 Comparison of the 17-year averaged (1998–2014) daily time series of (a) regionally averaged SST and (b) regionally averaged POC concentrations. The geographical positions of the regions are shown in Figs. 4a and 5a are explained in the text.

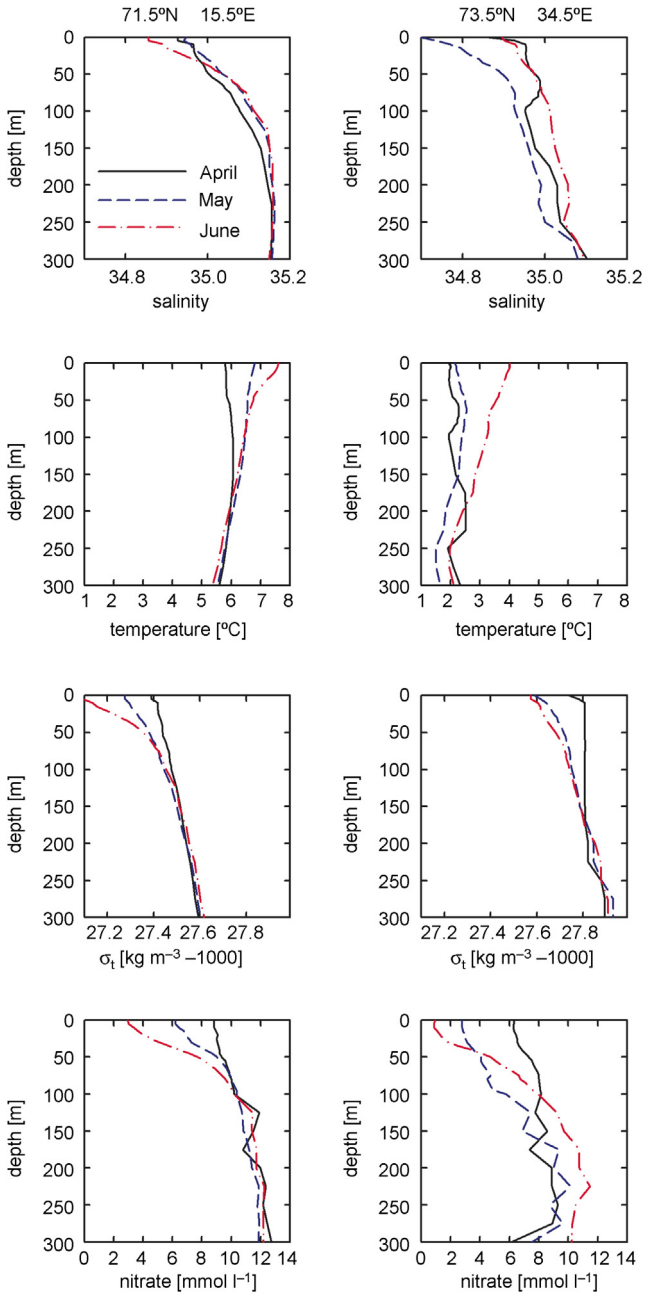

Figure 7 Comparison of the monthly climatology (based on WORLD OCEAN ATLAS 2013 version 2 objectively analyzed mean data on 1° grid from years 1995–2012) of water temperature, salinity, density $\sigma(t, s, 0)$, and nitrate concentration at grid points located within region 1 (left panel) and 2 (right panel).

and are lower than the annual maximum values in regions 2 and 3. In the coastal waters (region 4) the seasonal progression of POC cycle has a similar shape as in region 1, but it seems that higher POC concentrations are observed in coastal waters. Note, that the seasonal averages (May–August) of POC concentrations shown in Fig. 4e are significantly higher in the south-eastern part of the BS than in the western part of the study region. If we compare POC maps (Fig. 4) with SST and SLA maps (Figs. 2 and 3) we note that the region where seasonally averaged POC concentrations reach the spectacularly high values coincides with the area where the annual amplitude and standard deviation of SST as well as standard deviation of SLA are large. This suggests that the more variable thermal and dynamic environment, where vertical mixing of the water column is very intense, is also more prone to sustaining high production of POC particles.

Summarizing, the satellite POC concentrations in the open BS display seasonal variability that can be associated with the seasonal cycle in phytoplankton productivity and abundance. In the literature the Barents Sea has been described as a spring bloom system (Olsen et al., 2003; Rey, 1981). It has been shown that the exact timing of the phytoplankton bloom is somewhat variable and has significant regional variability throughout the Barents Sea. Usually the main bloom has been associated with the onset of seasonal stratification of the water column. The dominant algal group during the spring bloom are diatoms, and *Chaetoceros socialis* is often the most abundant species (Olsen et al., 2003; Rey, 1981). The concentrations of diatoms can reach up to several million cells per liter. When the silicate becomes limiting other algal groups such as flagellates take over. The most important flagellate species in the Barents Sea is *Phaeocyctis pouchetii*.

In order to derive a better understanding of the observed regional differences in the seasonal POC cycle in the BS we have plotted in Fig. 7 the vertical profiles of water temperature, salinity, density, and nitrate concentrations. These data represent climatology from WOA 2013 data sets for grid points located within regions 1 and 2. The lowest surface temperature in the upper part of the water column in both

regions is observed in April (we did not plot profiles for earlier months to improve the clarity of Fig. 7). Water salinity increases with depth, but generally water is less salty in region 2 than in region 1, while water temperature is lower in region 2 than in region 1. It is interesting to note that in April there is a small, but obvious decrease of salinity near the water surface in region 1 and 2, which translates to a decrease of water density that is more pronounced in region 2 than in region 1. It is also remarkable that water column density in region 2 is very well homogenized down till about 250 m, except for this small feature near the surface which is due to a decrease of water salinity. In region 2 in May, there is a further decrease of water salinity, which causes a decrease of water density and increases the stability of surface waters. This supports the notion that the inflow of melt water creates the opportunity for the onset of phytoplankton bloom. In May nitrate concentrations in region 2 are already significantly lower than in April (this decrease can be observed as deep as 120–150 m), which is consistent with our belief that significant primary production takes place here at this time of the year. In contrast to region 2, water column is weakly stratified in region 1 in April, but the mixed layer depth (defined by change in the water density, Monterey and Levitus, 1997) is still relatively deep (~150 m). In May surface water stratification increases, but if we look at the vertical profiles of nitrate concentrations, we can see that the change between April and May is smaller in region 1 and larger in region 2. This is in agreement with our observation that there is only small increase in the abundance of POC particles here in May.

Based on the presented data we suggest that the regional differences in the seasonal cycle of POC concentration to a large degree reflect regional differentiation in seasonal productivity and abundance of phytoplankton. These regional differences are determined by large scale air–sea interaction processes. Intense water column mixing during winter in the entire region pre-conditions it for the occurrence of intense seasonal phytoplankton blooms. The blooms start early in the study area 2, because the surface waters become stabilized when the low-salinity melt water is supplied. The fact that the water column is almost homogenous at the beginning of the spring, allows for efficient replenishing of nutrients at the time period when the bloom develops. At this time of the year the periods of calmer seas are alternating with stormy weather. Such conditions are very favorable for development of extreme phytoplankton blooms. The fact that the seasonal increase of POC concentration is observed later in study area 1 in comparison to study area 2 can be explained by lower supply of melt water in the area 1. Therefore, the initiation of the spring bloom in region 1 is delayed until the net heat flux is sufficient to stabilize the surface waters. However, the net heat flux in the spring also seems to favor more efficient warming of surface waters in region 2 than in region 1 (see Fig. 8). Note that according to NCEP convention negative heat flux indicates that the atmosphere is loosing and the ocean surface is gaining heat. Thus according to Fig. 8 in spring and summer (on average) more heat is transferred from the atmosphere to the ocean surface in region 2 than in region 1. In addition, the intensity of the spring blooms in region 2 is amplified by the fact that below the surface, the water column remains well mixed after the winter. Note that, since region 2 is located on the shelf with water depths of about 300 m or less, winter mixing reaches

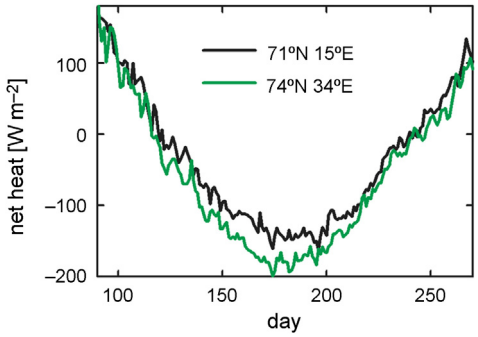

Figure 8 Comparison of the mean daily net heat flux at grid points located within region 1 and 2 (based on NCEP data from years 1998–2014 on sensible, latent, net shortwave and longwave radiation flux data).

the bottom water layer. This allows for efficient re-supply of nutrients from deep waters in winter and intermittent supply of nutrients in spring during storms. The main difference between region 1 and 2 is that region 1 is located in warmer AW waters in deeper ocean, and there is lower supply of low salinity waters. In addition, although there is an efficient mixing of warm advected water masses, water column does not appear to be as completely homogenous as in region 2. Phytoplankton biomass seems to increase in spring in response to seasonal warming of surface waters and this happens later than the onset of phytoplankton bloom in regions 2 and 3.

In addition to the seasonal cycle, satellite data allow us to trace the interannual variability of POC concentrations. This is shown in Fig. 9a, where regionally averaged May POC concentrations plotted as a function of the year have been compared. The highest POC concentrations are observed in year 2003. Interestingly, although the concentrations are generally lower in region 1 than in regions 2 and 3, nevertheless the patterns of interannual variability seem similar in all 3 regions. This is confirmed by scatter plots (Fig. 9b), that show statistically significant correlations between POC concentrations observed between regions 1 and 2 and between regions 1 and 3. In addition the seasonally (May–August) averaged POC concentrations are strongly influenced by the concentrations reached during the month when the maximum concentrations are observed. This is supported by the results summarized in Fig. 9c, where we can see a statistically significant correlation between May and seasonally averaged POC concentrations in regions 2 and 3. In region 1 the seasonally averaged POC concentrations correlate best with June POC concentrations. What is more, the interannual variability in POC concentrations can be linked to SST variability. We have analyzed different sets of data (heat fluxes, wind stress, air temperatures) and we have found out that the best, statistically significant correlation is observed between the minimum value of the regionally averaged SST in the winter season and the May POC concentrations (Fig. 9d). Correlations between April or May atmospheric or SST data and May POC concentrations were not statistically significant (not shown). This suggests that the interannual POC variability depends on winter pre-conditioning of the water masses. These could include more complete homogenization of the water column as well as production of more

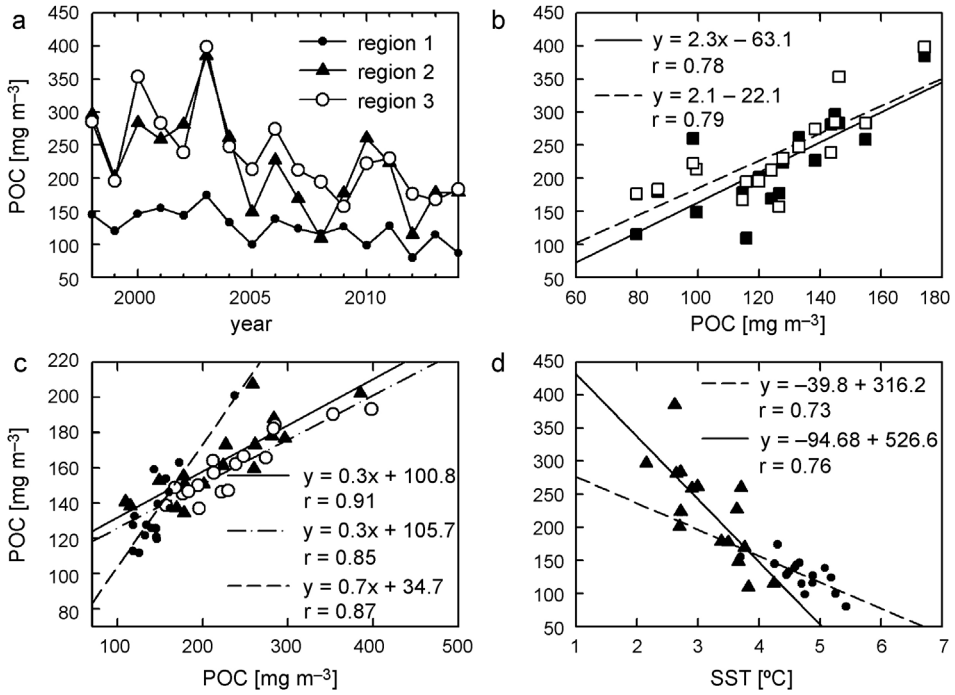

Figure 9 Interannual variability of POC concentration and SST in the study regions. (a) Time series regionally averaged of POC concentrations in the months of May in region 1 (black dots), 2 (black triangles) and 3 (open circles). (b) Relationships between the regionally averaged POC concentrations in May in different regions. Black squares and solid line are for region 2 plotted as a function of region 1, and open squares and dashed line are for region 3 versus region 1. Horizontal axis is for region 1. (c) Relationships between regional POC concentrations averaged over summer (May–August, shown on vertical axis) and the regional maximum monthly mean POC concentrations. Dashed line and dots are for POC concentrations in June in region 1, solid line and triangles are for POC concentrations in May in region 2, dash-dot-dash line and open circles are for POC concentrations in May in region 3. (d) Correlations between the regionally averaged POC concentrations in May and the regionally averaged annual minimum SST (dashed line and black dots are for region 1, solid line and triangles are for region 2).

sea ice in winter resulting in a better supply of melt water in the spring.

Because of the extremely high POC concentrations and efficient mixing of waters, the Barents Sea is potentially an important region for export of POC particles to deep waters. Note, that POC particles have low sinking velocities because their density is close to that of seawater. Traditionally, two processes have been attributed a major role for exporting POC. These are transport associated with the zooplankton ecosystem, and transport by gravitational settling of biogenic aggregates ballasted by heavy biomineral and lithogenic particles. Another potentially important mechanism for export of POC particles from surface waters is turbulent diffusion and mixing, in particular during energetic mixing episodes of surface waters in response to atmospheric forcing events (e.g., Stramska, 2010). This mechanism can play a particularly strong role in the Barents Sea.

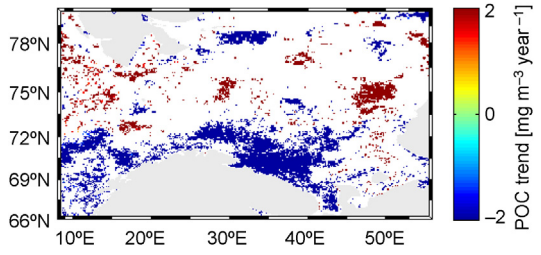

Figure 10 Map indicating pixels with statistically significant trend in surface POC concentrations ($p < 0.01$, 90% confidence level). Trend has been estimated using data from MODIS-Aqua (2003–2014).

Seasonally averaged POC concentrations can be used to investigate multiyear trends. We have tested if regional trends are statistically significant using data from MODIS-A (data from years 2003–2014). The results are presented in Fig. 10, where only pixels with statistically significant trends have been included. Trends of decreasing POC concentrations have been detected in few areas of the southern Barents Sea. This could be associated with less efficient mixing and more stable water masses in this polar province. It is generally expected that global climate change can slow the production of dense water masses due to less efficient creation of sea ice in this region. Increase in the SST has been confirmed by the analysis of the long-term SST data records. Note however that the results concerning POC trends need to be taken with caution and cannot be interpreted at this time as climate related change, because time series used in our calculations are too short for detection of climate trends.

4. Conclusions

Our main focus in this paper is in regional and seasonal variability of POC concentration in the region of the Barents

Sea. Since northern parts of the BS are covered by sea ice, our attention has been mostly on the southern part of the BS. Results presented in this paper have been based on ocean color satellite data supported by other interdisciplinary data sets available for research. The most important findings can be summarized in the following way.

- Seasonal increase in POC concentration in the southeastern Barents Sea is evident in May and is observed earlier in the year than in the southwestern side and in the neighboring waters of the Norwegian Sea. This is most likely associated with the stabilization of the surface waters by melt water beginning in April that allows for an early onset of phytoplankton bloom in the southeastern Barents Sea.
- In the southwestern edge of the Barents Sea and its vicinity, the seasonal increase of POC concentration is observed later in the year (end of May—June). This is likely associated with the fact that phytoplankton bloom in this area develops in response to water stratification taking place due to increased seasonal solar heating of surface waters. Seasonal increase of net heat flux gained by the ocean from the atmosphere and stabilization of the water column due to an increase in surface water temperature in this region is observed later in the year than the stabilization of surface waters in the southeastern Barents Sea by the advection of low salinity waters from melting sea ice.
- POC concentrations in the southeastern Barents Sea are among the highest observed in the global ocean. This can be linked to the fact that waters in this region become efficiently mixed during winters. The vertical mixing processes that take place during winters are important for transporting nutrient rich water to the surface, and this allows for high primary production in spring. In addition weak stratification of waters in May and June most likely allows for periodical replenishing the nutrients during storms and sustaining relatively high primary production and POC concentration through the summer months.
- Interannual variability of POC concentration in the open waters has been linked to lower SSTs observed in the winter season.
- In coastal waters the seasonal cycle of POC concentrations is not synchronized with the cycle observed in the open sea.
- We have shown that POC concentrations in the southern part of the Barents Sea tend to decrease in recent years. The decreasing trend has been detected with data from MODIS-Aqua from 2003 to 2014. This result needs to be taken with caution, as the ocean color time series are still too short to interpret this result as climate related trend.

Results presented in this paper strongly support the notion that seasonal restratification of the water column drives the changes in concentration of POC in surface waters from mid-winter lows to spring highs in the Barents Sea. In recent years there has been a renewed interest in Sverdrup's (1953) critical depth hypothesis (e.g., Behrenfeld, 2010; Chiswell, 2011). Conceptually, Sverdrup's hypothesis means that the balance between net phytoplankton production and the vertical mixing can determine the fate of phytoplankton populations in a variety of environments. Satellite data presented in our manuscript do not allow us to make calculations according to the model proposed by Sverdrup, since we do not have any data on grazing and community respiration. Nonetheless, our research supports the belief that mixing is critical for the temporal and spatial patterns observed in phytoplankton biomass in the Barents Sea.

Acknowledgments

The authors are grateful to all the persons involved in the programs providing free access to the data sets used in this study. The ocean color data were made available through the NASA Ocean Color Web (oceancolor.gsfc.nasa.gov/). The National Oceanic and Atmospheric (NOAA) Optimum Interpolation SST (OISST) Version 2 data set were made available by the NOAA Earth System Research Laboratory Physical Science Division (ESRL/PSD) and the meteorological data were obtained from the National Centers for Environmental Prediction and National Center for Atmospheric Research (NCEP/NCAR) Reanalysis Project at the NOAA/OAR/ESRL PSD (http://www.esrl.noaa.gov/psd/). World Ocean Atlas data (WOA 2013 version 2, www.nodc.noaa.gov/OC5/woa13/) were provided by the National Ocean and Atmospheric Administration (NOAA) National Centers for Environmental Information (NCEI). The altimeter data were processed by Ssalto/Duacs and distributed by AVISO, with support from Cnes (http://www.aviso). We would also like to thank Sebastian Meler from the IO PAN for help with data transfers.

Funding: This work was funded by the Norway Grants through the Polish-Norwegian Research Programme operated by the National Centre for Research and Development (NCBR contract No. 201985 entitled 'Application of in situ observations, high frequency radars, and ocean color, to study suspended matter, particulate carbon, and dissolved organic carbon fluxes in coastal waters of the Barents Sea'). Partial support for MS comes also from the statutory funds of the Institute of Oceanology of the Polish Academy of Sciences (IO PAN) and from the National Science Centre (NCN) in Poland through grant 2011/01/M/ST10/07728 'Global estimates of particulate organic carbon reservoir and export flux in the ocean based on satellite ocean color data'.

References

Ådlandsvik, B., Loeng, H., 1991. A study of the climatic system in the Barents Sea. Polar Res. 10 (1), 45—50, http://dx.doi.org/10.1111/j.1751-8369.1991.tb00633.x.

Årthun, M., Eldevik, T., Smedsrud, L.H., Skagseth, Ø., Ingvaldsen, R. B., 2012. Quantifying the influence of Atlantic heat on Barents Sea variability and retreat. J. Climate 25, 4736—4743.

Behrenfeld, M.J., 2010. Abandoning Sverdrup's critical depth hypothesis on phytoplankton blooms. Ecology 91 (4), 977—989, http://dx.doi.org/10.1890/09-1207.1.

Behrenfeld, M.J., O'Malley, R.T., Siegel, D.A., McClain, C.R., Sarmiento, J.L., Feldman, G.C., Milligan, A.J., Falkowski, P.G., Letelier, R.M., Boss, E.S., 2006. Climate-driven trends in contemporary ocean productivity. Nature 444 (7120), 752—755, http://dx.doi.org/10.1038/nature05317.

Bendat, J.S., Piersol, A.G., 2010. Random Data: Analysis and Measurement Procedures, 4th ed. Wiley, New Jersey, 640 pp.

Beszczynska-Möller, A., Fahrbach, E., Schauer, U., Hansen, E., 2012. Variability in Atlantic water temperature and transport at the entrance to the Arctic Ocean, 1997—2010. ICES J. Mar. Sci. 69 (5), 852—863, http://dx.doi.org/10.1093/icesjms/fss056.

Boyer, T.P., Antonov, J.I., Baranova, O.K., Coleman, C., Garcia, H.E., Grodsky, A., Johnson, D.R., Locarnini, R.A., Mishonov, A.V., O'Brien, T.D., Paver, C.R., Reagan, J.R., Seidov, D., Smolyar, I. V., Zweng, M.M., 2013. World Ocean Database 2013, NOAA Atlas NESDIS 72, S. Levitus, Ed., A. Mishonov, Technical Ed. Silver Spring, MD, http://dx.doi.org/10.7289/V5NZ85MT, 209 pp.

Campbell, J.W., Blaisdell, J.M., Darzi, M., 1995. Level-3 SeaWiFS Data Products: Spatial and Temporal Binning Algorithms. SeaWiFS Tech. Rep. Ser. 32, 73 pp.

Chiswell, S.M., 2011. Annual cycles and spring blooms in phytoplankton: don't abandon Sverdrup completely. Mar. Ecol. Prog. Ser. 443, 39–50, http://dx.doi.org/10.3354/meps09453.

Cole, H., Henson, S., Martin, A., Yool, A., 2012. Mind the gap: the impact of missing data on the calculation of phytoplankton phenology metrics. J. Geophys. Res.-Oceans 117 (C8), C08030, http://dx.doi.org/10.1029/2012JC008249.

Dmitrenko, I.A., Rudels, B., Kirillov, S.A., Aksenov, Y.O., Lien, V.S., Ivanov, V.V., Schauer, U., Polyakov, I.V., Coward, A., Barber, D.G., 2015. Atlantic water flow into the Arctic Ocean through the St. Anna Trough in the northern Kara Sea. J. Geophys. Res.-Oceans 120 (7), 5158–5178, http://dx.doi.org/10.1002/2015JC010804.

Doron, M., Babin, M., Mangin, A., Hembise, O., 2007. Estimation of light penetration, and horizontal and vertical visibility in oceanic and coastal waters from surface reflectance. J. Geophys. Res. 112 (C6), C06003, http://dx.doi.org/10.1029/2006JC004007.

Duforêt-Gaurier, L., Loisel, H., Dessailly, D., Nordkvist, K., Alvain, S., 2010. Estimates of particulate organic carbon over the euphotic depth from in situ measurements. Application to satellite data over the global ocean. Deep-Sea Res. Pt I 57 (3), 351–367, http://dx.doi.org/10.1016/j.dsr.2009.12.007.

Fasham, M., Ducklow, H.W., McKelvie, S.M., 1990. A nitrogen based model of plankton dynamics in the oceanic mixed layer. J. Mar. Res. 48 (3), 591–639.

Franz, B.A., Bailey, S.W., Werdell, P.J., McClain, C.R., 2007. Sensor-independent approach to the vicarious calibration of satellite ocean color radiometry. Appl. Optics 46 (22), 5068–5082, http://dx.doi.org/10.1364/AO.46.005068.

Furevik, T., 2001. Annual and interannual variability of Atlantic Water temperatures in the Norwegian and Barents Seas: 1980–1996. Deep-Sea Res. Pt I 48 (2), 383–404.

Gardner, W.D., Mishonov, A.V., Richardson, M.J., 2006. Global POC concentrations from in-situ and satellite data. Deep-Sea Res. Pt II 53 (5–7), 718–740, http://dx.doi.org/10.1016/j.dsr2.2006.01.029.

Good, S.A., Corlett, G.K., Remedios, J.J., Noyes, E.J., Llewellyn-Jones, D.T., 2007. The global trend in sea surface temperature from 20 years of Advanced Very High Resolution Radiometer Data. J. Climate 20, 1255–1264, http://dx.doi.org/10.1175/JCLI4049.1.

Guemas, V., Salas-Melia, D., 2008. Simulation of the Atlantic meridional overturning circulation in an atmosphere-ocean global coupled model. Part II: A weakening in a climate change experiment: a feedback mechanism. Clim. Dynam. 30 (7), 831–844, http://dx.doi.org/10.1007/s00382-007-0328-8.

Henson, S.A., Sarmiento, J.L., Dunne, J.P., Bopp, L., Lima, I., Doney, S.C., John, J., Beaulieu, C., 2010. Detection of anthropogenic climate change in satellite records of ocean chlorophyll and productivity. Biogeosciences 7 (2), 621–640, http://dx.doi.org/10.5194/bg-7-621-2010.

Hofmann, M., Worm, B., Rahmstorf, S., Schellnhuber, H.J., 2011. Declining ocean chlorophyll under unabated anthropogenic CO_2 emissions. Environ. Res. Lett. 6 (3), 1–7, http://dx.doi.org/10.1088/1748-9326/6/3/034035.

Jakowczyk, M., Stramska, M., 2014. Spatial and temporal variability of satellite-derived sea surface temperature in the Barents Sea. Int. J. Remote Sens. 35 (17), 6545–6560, http://dx.doi.org/10.1080/01431161.2014.958247.

Kirk, J.T.O., 1984. Dependence of relationship between inherent and apparent optical properties of water on solar altitude. Limnol. Oceanogr. 29 (2), 350–356.

Kirk, J.T.O., 1991. Volume scattering function, average cosines, and the underwater light field. Limnol. Oceanogr. 36 (3), 455–467.

Kivimäe, C., Bellerby, R.G.J., Fransson, A., Reigstad, M., Johannessen, T., 2010. A carbon budget for the Barents Sea. Deep-Sea Res. Pt I 57 (12), 1532–1542, http://dx.doi.org/10.1016/j.dsr.2010.05.006.

Kowalik, Z., Proshutinsky, A.Y., 1995. Topographic enhancement of tidal motion in the western Barents Sea. J. Geophys. Res.-Oceans 100 (C2), 2613–2637.

Le Provost, C., 2001. Ocean tides. In: Fu, L.-L., Cazenave, A. (Eds.), Satellite Altimetry and Earth Sciences: A Handbook of Techniques and Applications. Int. Geophys. Ser., vol. 69. Academic Press, San Diego, CA, pp. 267–304.

Lebedev, S., Kostyanoy, A.G., Ginzburg, A.I., Medvedev, D.P., Sheremet, N.A., Shauro, S.N., 2011. Satellite altimetry applications in the Barents and White seas. In: Vignudelli, S., Kostianoy, A.G., Cipollini, P., Benveniste, J. (Eds.), Coastal Altimetry. Springer-Verlag, Berlin, Heidelberg, 389–415.

Lee, Z.-P., Darecki, M., Carder, K.L., Davis, C.O., Stramski, D., Rhea, W.J., 2005a. Diffuse attenuation coefficient of downwelling irradiance: an evaluation of remote sensing methods. J. Geophys. Res. 110 (C2), C02017, http://dx.doi.org/10.1029/2004JC002573.

Lee, Z.-P., Du, K.P., Arnone, R., 2005b. A model for the diffuse attenuation coefficient of downwelling irradiance. J. Geophys. Res. 110 (C2), C02016, http://dx.doi.org/10.1029/2004JC002275.

Lee, Z.-P., Weidemann, A., Kindle, J., Arnone, R., Carder, K.L., Davis, C., 2007. Euphotic zone depth: its derivation and implication to ocean-color remote sensing. J. Geophys. Res. 112 (C3), C03009, http://dx.doi.org/10.1029/2006JC003802.

Lien, V.S., Trofimov, A.G., 2013. Formation of Barents Sea branch water in the northeastern Barents Sea. Polar Res. 32, 18905, http://dx.doi.org/10.3402/polar.v32i0.18905.

Lien, V.S., Vikebo, F.B., Skagseth, O., 2013. One mechanism contributing to co-variability of the Atlantic inflow branches to the Arctic. Nat. Commun. 4, 1488, http://dx.doi.org/10.1038/ncomms2505.

Luo, J.-J., Behera, S.K., Masumoto, Y., Yamagata, T., 2011. Impact of global ocean surface warming on seasonal-to-interannual climate prediction. J. Climate 24 (6), 1626–1646, http://dx.doi.org/10.1175/2010JCLI3645.1.

Marra, J.F., Dickey, T.D., Plueddemann, A.J., Weller, R.A., Kinkade, C.S., Stramska, M., 2015. Phytoplankton bloom phenomena in the North Atlantic Ocean and Arabian Sea. ICES J. Mar. Sci., http://dx.doi.org/10.1093/icesjms/fsu241.

Maslowski, W., Marble, D., Walczowski, W., Schauer, U., Clement, J. L., Semtner, A.J., 2004. On climatological mass, heat, and salt transports through the Barents Sea and Fram Strait from a Pan-Arctic coupled ice ocean model simulation. J. Geophys. Res. 109 (C3), C03032, http://dx.doi.org/10.1029/2001JC001039.

Merchant, C.J., LeBorgne, P., 2010. Retrieval of sea surface temperature from space, based on modeling of infrared radiative transfer: capabilities and limitations. J. Atmos. Ocean. Tech. 21 (11), 1734–1746, http://dx.doi.org/10.1175/JTECH1667.1.

Mobley, C.D., 1994. Light and Water. Radiative Transfer in Natural Waters. Academic Press, New York, 592 pp.

Monterey, G., Levitus, S., 1997. Seasonal variability of mixed layer depth for the World Ocean. NOAA Atlas, NESDIS 14, Washington, DC, 100 pp.

Morice, C.P., Kennedy, J.J., Rayner, N.A., Jones, P.D., 2012. Quantifying uncertainties in global and regional temperature change using an ensemble of observational estimates: the HadCRUT4 data set. J. Geophys. Res. 117 (D8), D08101, http://dx.doi.org/10.1029/2011JD017187.

Nerem, R.S., Chambers, D.P., Choe, C., Mitchum, G.T., 2010. Estimating mean sea level change from the TOPEX and Jason altimeter missions. Mar. Geod. 33 (Suppl. 1), 435–446, http://dx.doi.org/10.1080/01490419.2010.491031.

Olsen, A., Johannessen, T., Rey, F., 2003. On the nature of the factors that control spring bloom development at the entrance to the Barents Sea and their interannual variability. Sarsia 88 (6), 379–393, http://dx.doi.org/10.1080/00364820310003145.

O'Reilly, J.E., Maritorena, S., Mitchell, B.G., Siegel, D.A., Carder, K.L., Garver, S.A., Kahru, M., McClain, C.R., 1998. Ocean color chlorophyll algorithms for SeaWiFS. J. Geophys. Res. 103 (C11), 24937–24953, http://dx.doi.org/10.1029/98JC02160.

O'Reilly, J.E., Maritorena, S., Siegel, D.A., O'Brien, M.C., Toole, D., Mitchell, B.G., Kahru, M., Chavez, F.P., Strutton, P., Cota, G.F., Hooker, S.B., McClain, C.R., Carder, K.L., Muller-Karger, F., Harding, L., Magnuson, A., Phinney, D., Moore, G.F., Aiken, J., Arrigo, K.R., Letelier, R., Culver, M., 2000. Ocean color chlorophyll *a* algorithms for SeaWiFS, OC2 and OC4: Version 4. NASA Technical Memo 2000-206892, vol. 11. pp. 9–27.

Oziel, L., Sirven, J., Gascard, J.-C., 2016. The Barents Sea frontal zones and water masses variability (1980–2011). Ocean Sci. 12 (1), 169–184, http://dx.doi.org/10.5194/os-12-169-2016.

Padman, L., Erofeeva, S., 2004. A barotropic inverse tidal model for the Arctic Ocean. Geophys. Res. Lett. 31 (2), L02303, http://dx.doi.org/10.1029/2003GL019003.

Racault, M.-F., Sathyendranath, S., Platt, T., 2014. Impact of missing data on the estimation of ecological indicators from satellite ocean-colour time-series. Remote Sens. Environ. 152, 15–28, http://dx.doi.org/10.1016/j.rse.2014.05.016.

Rey, F., 1981. The development of the spring phytoplankton outburst at selected sites off the Norwegian coast. In: Sætre, R., Mork, M. (Eds.), The Norwegian Coastal Current. Univ. Bergen, 649–680.

Reynolds, R.W., Smith, T.M., Liu, C., Chelton, D.B., Casey, K.S., Schlax, M.G., 2007. Daily high-resolution-blended analyses for sea surface temperature. J. Climate 20 (22), 5473–5496, http://dx.doi.org/10.1175/2007JCLI1824.1.

Rudels, B., Jones, E.P., Schauer, U., Eriksson, P., 2004. Atlantic sources of the Arctic Ocean surface and halocline waters. Polar Res. 23 (2), 181–208, http://dx.doi.org/10.1111/j.1751-8369.2004.tb00007.x.

Schauer, U., Beszczynska-Möller, A., Walczowski, W., Fahrbach, E., Piechura, J., Hansen, E., 2008. Variation of measured heat flow through the Fram Strait between 1997 and 2006. In: Dickson, R.R., Meincke, J., Rhines, P. (Eds.), Arctic Subarctic Ocean Fluxes: Defining the Role of the Northern Seas in Climate. Springer, New York, 65–85.

Schauer, U., Loeng, H., Rudels, B., Ozhigin, V.K., Dieck, W., 2002. Atlantic water flow through the Barents and Kara seas. Deep-Sea Res. Pt I 49 (12), 2281–2298, http://dx.doi.org/10.1016/S0967-0637(02)00125-5.

Semeneov, V.A., Park, W., Latif, M., 2009. Barents Sea inflow shutdown: a new mechanism for rapid climate changes. Geophys. Res. Lett. 36 (14), L14709, http://dx.doi.org/10.1029/2009GL038911.

Serreze, M., Barrett, A., Slater, A., Steele, M., Zhang, J., Trenberth, K., 2007. The large-scale energy budget of the Arctic. J. Geophys. Res. 112 (D11), 1438–1445, http://dx.doi.org/10.1029/2006JD008230.

Siegel, D.A., Behrenfeld, M.J., Maritorena, S., McClain, C.R., Antoine, D., Bailey, S.W., Bontempi, P.S., Boss, E.S., Dierssen, H.M., Doney, S.C., Eplee, R.E., Evans, R.H., Feldman, G.C., Fields, E., Franz, B.A., Kuring, N.A., Mengelt, C., Nelson, N.B., Patt, F.S., Robinson, W.D., Sarmiento, J.L., Swan, C.M., Werdell, P.J., Westberry, T.K., Wilding, J.G., Yoder, J.A., 2013. Regional to global assessments of phytoplankton dynamics from the SeaWiFS mission. Remote Sens. Environ. 135, 77–91, http://dx.doi.org/10.1016/j.rse.2013.03.025.

Skjelvan, I., Olsen, A., Anderson, L.G., Bellerby, R.G.J., Falck, E., Kasajima, Y., Kivimae, C., Omar, A., Rey, F., Olsson, K.A., Johannessen, T., Heinze, C., 2005. A review of the biogeochemistry of the Nordic Seas and Barents Sea. In: Drange, H., Dokken, T., Furevik, T., Gerdes, R., Berger, W. (Eds.), The Nordic Seas: An Integrated Perspective Oceanography, Climatology and Modelling. American Geophysical Union, Washington, DC, 157–175.

Smedsrud, L.H., Esau, I., Ingvaldsen, R.B., Eldevik, T., Haugan, P.M., Li, C., Lien, V.S., Olsen, A., Omar, A.M., Otterå, O.H., Risebrobakken, B., Sandø, A.B., Semenov, V.A., Sorokina, S.A., 2013. The role of the Barents Sea in the Arctic climate system. Rev. Geophys. 51 (3), 415–449, http://dx.doi.org/10.1002/rog.20017.

Stramska, M., 2005. Interannual variability of seasonal phytoplankton blooms in the north polar Atlantic in response to atmospheric forcing. J. Geophys. Res. 110 (C5), C05016, http://dx.doi.org/10.1029/2004JC002457.

Stramska, M., 2010. The diffusive component of particulate organic carbon export in the North Atlantic estimated from SeaWiFS ocean color. Deep-Sea Res. Pt I 57 (2), 284–296, http://dx.doi.org/10.1016/j.dsr.2009.11.007.

Stramska, M., 2014. Particulate organic carbon in the surface waters of the North Atlantic: spatial and temporal variability based on satellite ocean colour. Int. J. Remote Sens. 35 (13), 4717–4738, http://dx.doi.org/10.1080/01431161.2014.919686.

Stramska, M., Cieszyńska, A., 2015. Ocean colour estimates of particulate organic carbon reservoirs in the global ocean – revisited. Int. J. Remote Sens. 36 (14), 3675–3700, http://dx.doi.org/10.1080/01431161.2015.1049380.

Stramska, M., Dickey, T.D., 1994. Modeling phytoplankton dynamics in the northeast Atlantic during the initiation of the spring bloom. J. Geophys. Res. 99 (c5), 10241–10253, http://dx.doi.org/10.1029/93JC03378.

Stramska, M., Dickey, T.D., Plueddemann, A., Weller, R., Langdon, C., Marra, J., 1995. Bio-optical variability associated with phytoplankton dynamics in the North Atlantic Ocean during spring and summer of 1991. J. Geophys. Res. 100 (C4), 6621–6632, http://dx.doi.org/10.1029/94JC01447.

Stramska, M., Frye, D., 1997. Dependence of apparent optical properties on solar altitude: experimental results based on mooring data collected in the Sargasso Sea. J. Geophys. Res. 102 (C7), 15679–15691, http://dx.doi.org/10.1029/97JC00886.

Stramski, D., Reynolds, R.A., Babin, M., Kaczmarek, S., Lewis, M.R., Röttgers, R., Sciandra, A., Stramska, M., Twardowski, M.S., Franz, B.A., Claustre, H., 2008. Relationships between the surface concentration of particulate organic carbon and optical properties in the Eastern South Pacific and Eastern Atlantic Oceans. Biogeosciences 5, 171–201, http://dx.doi.org/10.5194/bg-5-171-2008.

Sverdrup, H.U., 1953. On conditions for the vernal blooming of phytoplankton. J. Con. Cons. Perm. Int. Explor. Mer. 18 (3), 287–295.

Świrgoń, M., Stramska, M., 2015. Comparison of in situ and satellite ocean color determinations of particulate organic carbon concentration in the global ocean. Oceanologia 57 (1), 25–31, http://dx.doi.org/10.1016/j.oceano.2014.09.002.

Terziev, F.S., Girduk, G.V., Zykova, G.G., Dzhenyuk, S.L. (Eds.), 1990. Hydrometeorology and Hydrochemistry of the Seas of the USSR, vol. 1, Barents Sea, Issue 1, Hydrometerologicla Conditions. Hydrometeoizdat, Leningrad (in Russian).

Tett, P., Edwards, A., 1984. Mixing and plankton: an interdisciplinary theme in oceanography. Oceanogr. Mar. Biol. 22, 99–123.

van de Poll, W.H., Kulk, G., Timmermans, K.R., Brussaard, C.P.D., van der Woerd, H.J., Kehoe, M.J., Mojica, K.D.A., Visser, R.J.W., Rozema, P.D., Buma, A.G.J., 2013. Phytoplankton chlorophyll *a* biomass, composition, and productivity along a temperature and stratification gradient in the northeast Atlantic Ocean. Biogeosciences 10, 4227–4240, http://dx.doi.org/10.5194/bg-10-4227-2013.

Volkov, D.L., Landerer, F.W., Kirillov, S.A., 2013. The genesis of sea level variability in the Barents Sea. Cont. Shelf Res. 66, 92–104, http://dx.doi.org/10.1016/j.csr.2013.07.007.

Volkov, D.L., Pujol, M.-I., 2012. Quality assessment of a satellite altimetry data product in the Nordic, Barents, and Kara seas. J. Geophys. Res. 117 (C3), C03025, http://dx.doi.org/10.1029/2011JC007557.

Wassmann, P., Reigstad, M., Haug, T., Rudels, B., Carroll, M.L., Hop, H., Gabrielsen, G.W., Falk-Petersen, S., Denisenko, S.G., Arashkevich, E., Slagstad, D., Pavlova, O., 2006. Food webs and carbon flux in the Barents Sea. Prog. Oceanogr. 71 (2–4), 232–287, http://dx.doi.org/10.1016/j.pocean.2006.10.003.

Woźniak, S.B., 2014. Simple statistical formulas for estimating biogeochemical properties of suspended particulate matter in the southern Baltic Sea potentially useful for optical remote sensing applications. Oceanologia 56 (1), 7–39, http://dx.doi.org/10.5697/oc.56-1.007.

Woźniak, S.B., Meler, J., Lednicka, B., Zdun, A., Stoń-Egiert, J., 2011. Inherent optical properties of suspended particulate matter in the southern Baltic Sea. Oceanologia 53 (3), 691–729, http://dx.doi.org/10.5697/oc.53-3.691.